White Rose Research Online

eprints@whiterose.ac.uk
https://eprints.whiterose.ac.uk
Universities of Leeds, Sheffield and York

Deposited via The University of Leeds.

White Rose Research Online URL for this paper:
https://eprints.whiterose.ac.uk/id/eprint/153115/

Version: Accepted Version

Article:
Capel Berdiell, I, Farmiloe, SE, Kulmaczewski, R et al. (2019) Molecular Squares, Coordination Polymers and Mononuclear Complexes Supported by 2,4-Dipyrazolyl-6H-1,3,5-triazine and 4,6-Dipyrazolylpyrimidine Ligands. Dalton Transactions: an international journal of inorganic chemistry, 46. pp. 17310-17320. ISSN: 1477-9226

https://doi.org/10.1039/C9DT04003J

© The Royal Society of Chemistry. This is an author produced version of a paper published in Dalton Transactions. Uploaded in accordance with the publisher's self-archiving policy.

Reuse
Items deposited in White Rose Research Online are protected by copyright, with all rights reserved unless indicated otherwise. They may be downloaded and/or printed for private study, or other acts as permitted by national copyright laws. The publisher or other rights holders may allow further reproduction and re-use of the full text version. This is indicated by the licence information on the White Rose Research Online record for the item.

Takedown
If you consider content in White Rose Research Online to be in breach of UK law, please notify us by emailing eprints@whiterose.ac.uk including the URL of the record and the reason for the withdrawal request.

UNIVERSITY OF LEEDS
University of Sheffield
UNIVERSITY of York

Molecular Squares, Coordination Polymers and Mononuclear Complexes Supported by 2,4-Dipyrazolyl-6*H*-1,3,5-triazine and 4,6-Dipyrazolylpyrimidine Ligands†‡

Izar Capel Berdiell,[a] Sarah E. Farmiloe,[a] Rafal Kulmaczewski[a] and Malcolm A. Halcrow*[,a]

The $Fe[BF_4]_2$ complex of 2,4-di(pyrazol-1-yl)-6*H*-1,3,5-triazine (L^1) is a high-spin molecular square, $[\{Fe(L^1)\}_4(\mu\text{-}L^1)_4][BF_4]_8$, whose crystals also contain the unusual $HPzBF_3$ (HPz = pyrazole) adduct. Three other 2,4-di(pyrazol-1-yl)-6*H*-1,3,5-triazine derivatives with different pyrazole substituents (L^2-L^4) are unstable in the presence of first row transition ions, but form mononuclear, polymeric or molecular square complexes with silver(I). Most of these compounds involve *bis*-bidentate di(pyrazolyl)triazine coordination, which is unusual for that class of ligand, and the molecular squares encapsulate one or two BF_4^-, ClO_4^- or SbF_6^- ions through combinations of anion...π, Ag...X and/or C–H...X (X = O or F) interactions. Treatment of $Fe[NCS]_2$ or $Fe[NCSe]_2$ with 4,6-di(pyrazol-1-yl)-2*H*-pyrimidine (L^5) or its 2-methyl and 2-amino derivatives (L^6 and L^7) yields mononuclear $[Fe(NCE)_2L_2]$ and/or the 1D coordination polymers *catena*-$[Fe(NCE)_2(\mu\text{-L})]$ (E = S or Se, L = L^5-L^7). Alcohol solvates of isomorphous $[Fe(NCS)_2L_2]$ and $[Fe(NCSe)_2L_2]$ compounds show different patterns of intermolecular hydrogen bonding, reflecting the acceptor properties of the anion ligands. These iron compounds are all high-spin, although annealing solvated crystals of $[Fe(NCSe)_2(L^5)_2]$ affords a new phase exhibiting an abrupt, low-temperature spin transition. *Catena*-$[Fe(H_2O)_2(\mu\text{-}L^5)][ClO_4]_2$ is a coordination polymer of alternating *cis* and *trans* iron centres.

Introduction

Ditopic or polytopic ligands constructed around a central di-, tri- or tetra-azinyl scaffold are useful synthons for assembling arrays of metal centres into controlled topologies.[1-5] Larger polychelate ligands with pyridazinyl or pyrimidyl spacers have been designed to yield 2D grid complexes,[2,3] while divergent ligands centred on 1,3,5-triazinyl rings are important components in 3D coordination cages[4] or MOF structures.[5-7] The number and disposition of N atoms in the polyazine core influences electronic or magnetic interactions between metal ions which bind directly to those N donors.[2] Triazinyl ligands have the added feature of the π-acidity of the 1,3,5-triazine ring, which leads it to form strong anion...π interactions in the solid state.[8] This property has been exploited to introduce donor:acceptor functionality into triazine-containing MOFs.[6,7]

During our studies of tridentate ligands for spin-crossover molecular materials,[9] we discovered a family of heterometallic coordination polymer gels formed by adding silver salts to homoleptic $[M(tpt)_2]^{2+}$ (M = Fe, Co, Ni; tpt = 2,4,6-tri(pyrazol-1-yl)-1,3,5-triazine) precursors.[10] The gelation reflects the ability of the tpt ligand to chelate to two metal ions simultaneously through its triazinyl and pyrazolyl N-donors, forming robust networks of coordination polymer chains. As an extension of this chemistry we examined the coordination chemistry of other poly(pyrazoly)-1,3,5-triazine and poly(pyrazolyl)-pyrimidine derivatives, including those shown in Scheme 1. While none of these gave rise to functional metallogels they have yielded a variety of crystalline metal/organic assembly structures, some of which are described here.[10,11]

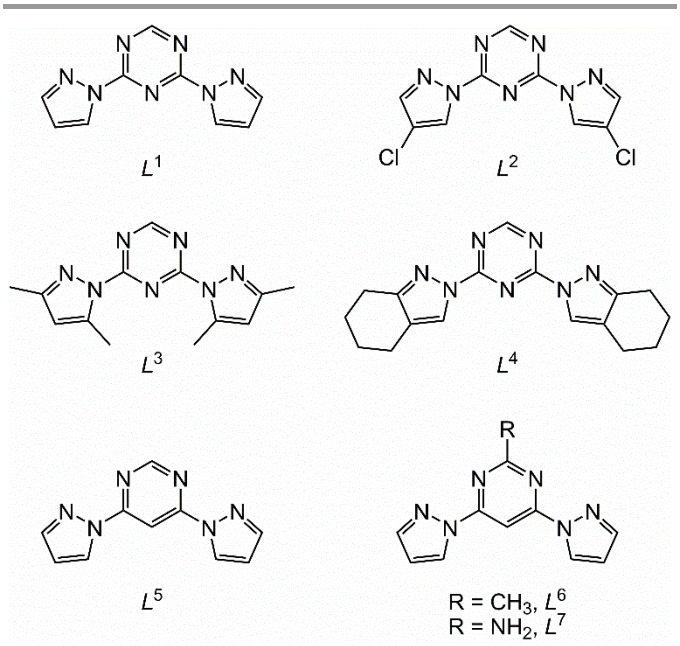

Scheme 1. The ligands referred to in this work.

[a] *School of Chemistry, University of Leeds, Woodhouse Lane, Leeds, UK LS2 9JT. E-mail: m.a.halcrow@leeds.ac.uk.*

† Electronic Supplementary Information (ESI) available: synthetic procedures and characterisation data for L^2-L^4; crystallographic data, refinement details, Figures and Tables for the ligand and complex structures; and additional solid and solution phase characterisation data. CCDC 1550948 and 1957573-1957592. For ESI and crystallographic data in CIF or other electronic format see DOI: 10.1039/x0xx00000x

‡ Data supporting this study are available at http://doi.org/10.5518/###.

While 2,4-dipyrazolyl-1,3,5-triazines are well-known ligands for *d*- and *f*-block metals, nearly all known examples bear additional amino, alkoxy or pyrazolyl substituents at the *C*6 position.[10,12-14] Analogues with an unprotected triazinyl *C*6 atom have been rarely studied, which may reflect their increased sensitivity to metal-promoted hydrolysis.[15] Of the 2,4-dipyrazolyl-6*H*-1,3,5-triazine derivatives in Scheme 1 only L^1 has been reported previously, as a silver(I) coordination polymer.[14] The parent 4,6-dipyrazolylpyrimidine ligand L^5 has been used as a bridging ligand in bimetallic organometallic compounds,[16,17] and as a probe for fluxional behaviour in some mononuclear chelate complexes.[17,18] A series of $[M_4(\mu\text{-L})_4]^{4+}$ (M = Cu^+ or Ag^+; L = L^5-L^7 or a related ligand) molecular squares have also been investigated by Manzano *et al*.[19-21] These adopt saddle-shaped conformations, and bind anions or aromatic solvents in their cavities through hydrophobic and (for $[Cu_4(\mu\text{-}L^7)_4]^{4+}$) hydrogen-bonding interactions. An Ag_4 molecular square supported by a 4,6-di(pyridyl)pyrimidine *bis*-chelate has also been described, although no anion encapsulation was noted in that case.[22]

The first part of this report describes an unusual $[Fe^{II}_4]^{8+}$ metallacycle supported by L^1, and $[Ag^{I}_4]^{4+}$ molecular squares and other silver complexes containing the new ligands L^2-L^4. These exhibit different geometries of anion...π interactions, which are typical of triazinyl host:guest assemblies. The second part of the paper includes iron(II) complexes of L^5-L^7, which we investigated as components in coordination polymers with potential for spin-crossover activity.[23,24]

Results and Discussion

Ligands L^1 and L^5-L^7 were prepared by the literature syntheses.[14,20,25] The new ligands L^2-L^4 were obtained by analogous procedures to that for L^1, by treating 2,4-dichloro-1,3,5-triazine with 2 equiv of the appropriate pyrazole in tetrahydrofuran, in the presence of sodium hydride base. Moderate yields of 41-62 % of NMR-pure products were obtained, after purification by chromatography if required.

Crystals of L^2·MeCN, L^4·2$CHCl_3$ and L^7 were characterised by X-ray diffraction. The conformation of the *tris*-heterocycles is the same in each case, with *anti* and (approximately) coplanar orientations of the pyrazolyl and azinyl rings. Two polymorphs of L^7 were distinguished in the monoclinic *C*2/*c* and orthorhombic $P2_12_12_1$ space groups, although the latter diffracted too weakly for a meaningful anisotropic structure refinement (Table S1). The asymmetric unit of L^4·2$CHCl_3$ (triclinic, $P\overline{1}$) contains two crystallographically unique L^4 molecules, which are related by an approximate non-crystallographic inversion centre. The chloroform molecules in that crystal donate bifurcated, chelating C–H...N interactions to pairs of L^4 pyrazolyl and triazinyl N atoms (Figure S6).

Despite many attempts, only one complex of L^1-L^4 with a divalent transition ion was obtained in analytical purity. That may reflect the aforementioned sensitivity of 1,3,5-triazines to metal-promoted hydrolysis.[10,15] The isolated complex had the empirical formula $[Fe(L^1)_2][BF_4]_2$ by microanalysis, but was revealed crystallographically to be tetrameric $[BF_4\subset\{Fe(L^1)\}_4(\mu\text{-}L^1)_4][BF_4]_7$·5.9MeCN·0.5($C_3H_4N_2BF_3$) (triclinic, $P\overline{1}$; Figure 1). The approximately square $[\{Fe(L^1)\}_4(\mu\text{-}L^1)_4]^{8+}$ core is supported by *bis*-bidentate L^1 ligands, with Fe…Fe distances of 6.5230(9)-6.6847(9) Å. Each iron atom is also bound by another bidentate L^1 ligand, in a *mer* six-coordinate geometry. The symmetry of the molecule is lowered from S_4 to C_1 by the peripheral L^1 ligand at Fe(3), which has a *transoid* rather than *cisoid* disposition with respect to its neighbour $[FeL^1]^{2+}$ vertices. The Fe–N distances in the molecule show some variation, but are consistent with high-spin iron(II) centres (Table S5).

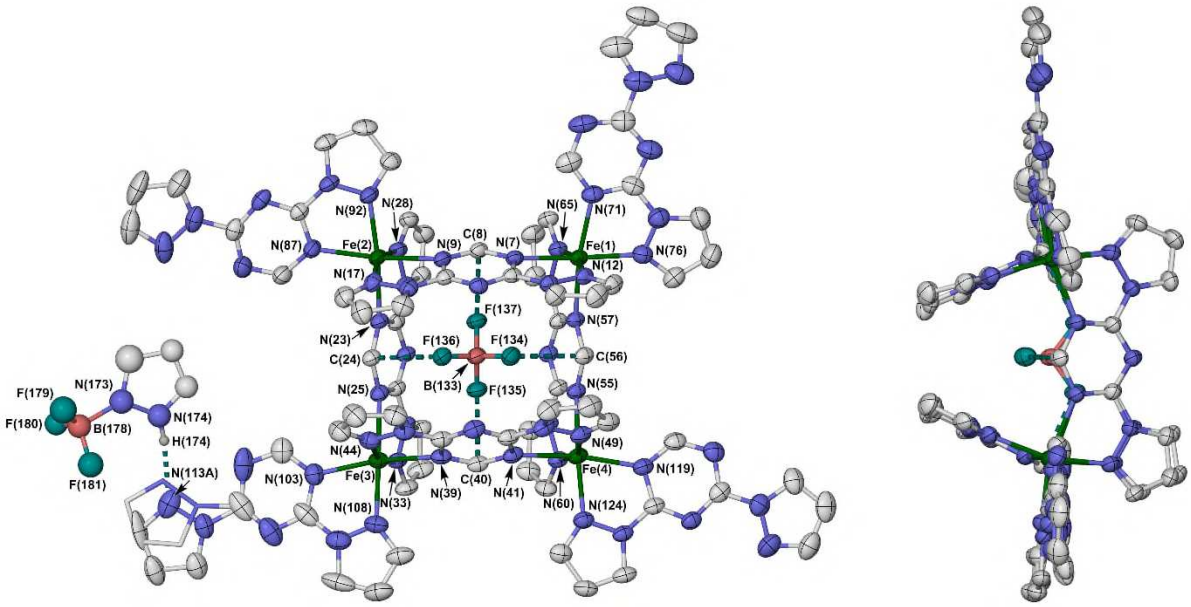

Figure 1 Two views of the $\{[BF_4\subset[\{Fe(L^1)\}_4(\mu\text{-}L^1)_4]\cdot0.5(C_3H_4N_2BF_3)\}^{7+}$ assembly in **1**·5.9MeCN·0.5($C_3H_4N_2BF_3$) with selected atom numbering. Atoms are drawn with 50 % displacement ellipsoids, except the minor orientation of the disordered pyrazolyl substituent which is de-emphasised for clarity, and all H atoms are omitted. Anion...π contacts involving the encapsulated BF_4^- ion are marked, but intermolecular interactions to the periphery of the metallacycle are not shown (Figure S11). The 0.5($C_3H_4N_2BF_3$) moiety is omitted from the right-hand view. Colour code: C, white; B, pink; F, cyan; Fe, green; N, blue.

A BF_4^- ion is encapsulated at the centre of the assembly, whose F atoms each form a close contact to the *C*6 atom of a different, π-acidic triazinyl ring (Figure 1). The F…C distances are 2.604(4)-2.642(4) Å, which are short contacts for an anion…π interactions to a 1,3,5-triazine ring.[8] Another unusual feature is the half-occupied (1*H*-pyrazole)→BF_3 adduct in the lattice (Figure 1), which may arise from pyrazole formed by partial hydrolysis of L^1 during the slow crystallization process;[10,26] there was no detectable pyrazole impurity in the ligand used to prepare the complex. While this is only the second observation of a pyrazole→BF_3 adduct, its dimensions are in excellent agreement with the literature example¶.[27]

In addition to the encapsulated BF_4^- ion, each bridging L^1 ligand forms a second dipole...dipole interaction to an exogenous species in the lattice which is not shown in Figure 1. This is either an additional anion... π interaction[8] or, in one case, a comparable *n*...π contact to a part-occupied acetonitrile molecule (Figure S11).[28] Two of the terminal L^1 ligands also accept anion... π interactions at their triazinyl rings. None of these peripheral interactions leads to bridging between the complex molecules in lattice. However, neighbouring cations do interact through intermolecular π...π interactions between their pendant pyrazolyl rings (Figure S13).

While the strongest peaks are derived from $[Fe(L^1)_2]^{2+}$, the ion $[Fe_4(L^1)_8(BF_4)_6]^{2+}$ (*m*/*z* = 1225) is clearly visible in the electrospray mass spectrum of that compound (Figure S14). That formula corresponds to the stoichiometry of the anion... π interactions observed in the crystal (Figure S11), although the significance of that observation is unclear. Few other higher-nuclearity species are present in the spectrum, which all contain sodium and/or formate from the spectrometer calibrant and so are artefacts of the measurement. Hence the $[Fe_4(L^1)_8]^{8+}$ assembly exists in solution, possibly in equilibrium with monomeric $[Fe(L^1)_2]^{2+}$ but not with other large assemblies. Magnetic susceptibility data confirm that $[\{Fe(L^1)\}_4(\mu\text{-}L^1)_4][BF_4]_8$ is high-spin in the solid state between 5-300 K, and between 237-343 K in CD_3CN solution (Figure S16).

The only previously reported complex of L^1 is $[Ag(\mu\text{-}L^1)]BF_4$, a 1D coordination polymer.[14] Silver complexes of L^2-L^4 also proved tractable, and crystallised in different aggregation states. The $AgClO_4$ complex of L^2 was crystallised from nitromethane and acetonitrile, yielding the 1D coordination polymers $[Ag(\mu\text{-}L^2)]ClO_4$ and $[Ag(NCMe)(\mu\text{-}L^2)]ClO_4$ respectively (both monoclinic, $P2_1/n$). Both complexes are zig-zag chain structures supported by *bis*-bidentate L^2 ligands, with a longer Ag...$OClO_3$ contact of 2.643(4)-2.670(2) Å. The silver ion in $[Ag(\mu\text{-}L^2)]ClO_4$ has an intermediate five-coordinate geometry [τ = 0.50],[29] while the additional ligand in the acetonitrile adduct gives that a distorted octahedral structure (Figure 2). That geometry change leads to a concertina-like contraction of the polymer chain, as evidenced by the dihedral angle between the bridging ligands at each silver vertex (Ψ), which is 107.22(4)° for $[Ag(\mu\text{-}L^2)]ClO_4$, and 77.04(4)° for $[Ag(NCMe)(\mu\text{-}L^2)]ClO_4$. The zig-zag topology of these coordination polymers contrasts with almost perfectly linear geometry adopted by $[Ag(\mu\text{-}L^1)]BF_4$.[14]

The perchlorate ions in both compounds lie in the clefts of the zig-zagging chains, forming an anion... π contact to a triazinyl C atom as well as the aforementioned Ag...O interaction. This is a weak intra-chain interaction in $[Ag(NCMe)(\mu\text{-}L^2)]ClO_4$, which packs as discrete polymer chains in the lattice (Figure 2). However, the anions in more open $[Ag(\mu\text{-}L^2)]ClO_4$ instead form a shorter inter-chain anion... π contact, linking those chains into two dimensions in the crystal (Figure S19).

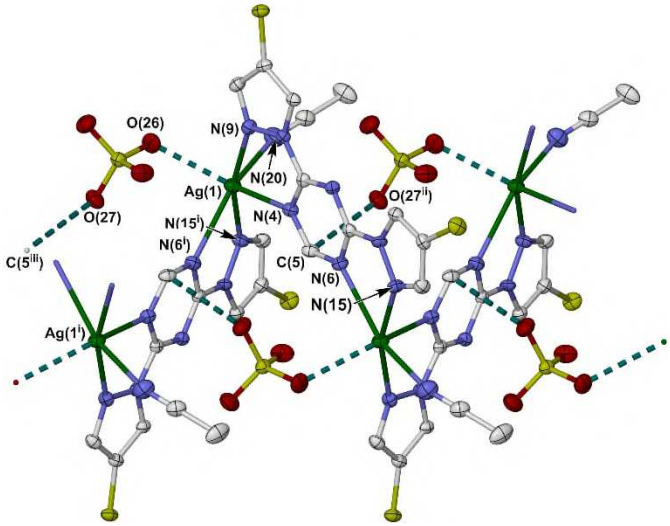

Figure 2 Section of the coordination polymer $[Ag(NCMe)(\mu\text{-}L^2)]ClO_4$. Atoms are drawn with 50 % displacement ellipsoids and H atoms are omitted for clarity. Colour code: C, white; Cl, yellow; Fe, green; N, blue; O, red. Symmetry codes: (i) $^1/_2-x$, $-^1/_2+y$, $^1/_2-z$; (ii) *x*, 1+*y*, *z*; (iii) *x*, –1+*y*, *z*.

The acetonitrile ligand in the solvated complex is labile, since the dried compound gave elemental analyses of approximate formula $[Ag(NCMe)_{0.25}(L^2)]ClO_4$. That may reflect that desolvation of $[Ag(NCMe)(\mu\text{-}L^2)]ClO_4$ can occur without otherwise changing the connectivity of the material.

In contrast, $AgClO_4$ adducts of more sterically crowded L^3 and L^4 yield molecular squares when crystallised from nitromethane. Needle and cubic morphologies of $[Ag_4(\mu\text{-}L^3)_4][ClO_4]_4$ co-crystallised under these conditions, which were respectively solvated (monoclinic, *C*2/*c*) and unsolvated (tetragonal, $P\bar{4}2_1c$) forms of the same cyclic tetramer. The solvate $[Ag_4(\mu\text{-}L^4)_4][ClO_4]_4{\cdot}MeNO_2$ (monoclinic, *C*2/*c*) was also crystallographically characterised, although that complex was not obtained in analytical purity. The silver ions in these metallacycles are four-coordinate, or [4+1]-coordinate with a long Ag...$OClO_3$ contact. Other differences between the structures involve the degree of canting of the "molecular square" assemblies, and the anion... π interactions present.

$[Ag_4(\mu\text{-}L^3)_4][ClO_4]_4$ and $[Ag_4(\mu\text{-}L^4)_4][ClO_4]_4{\cdot}MeNO_2$ have similar saddle-shaped conformations with exact, or approximate, S_4 symmetry (Figure 3, top and Figures S27-S30). These $[Ag_4(\mu\text{-}L)_4]^{4+}$ hosts contain two disordered ClO_4^- ions, each sandwiched between a pair of triazine rings by one or two anion... π and C–H...O contacts. This molecular and supramolecular geometry resembles those of previously reported $[Cu_4(\mu\text{-}L^5)_4]X_4$ (X = BF_4^- or PF_6^-) molecular squares.[19,20] However, solvated $[Ag_4(\mu\text{-}L^3)_4][ClO_4]_4{\cdot}3.2MeNO_2{\cdot}1.2H_2O$ has a more compact, canted geometry allowing it to bind just one ClO_4^- ion near centre of its cavity (Figure 3, bottom). This guest

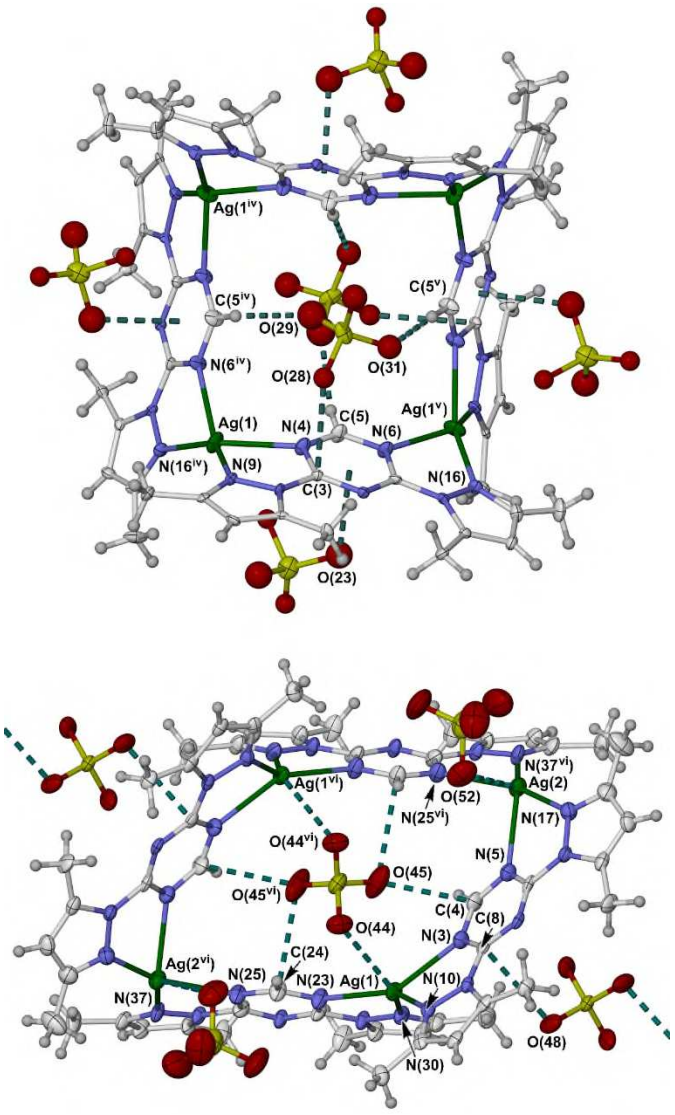

Figure 3 Comparison of the molecular square/anion assemblies in $[Ag_4(\mu\text{-}L^3)][ClO_4]_4$ (top) and $[Ag_4(\mu\text{-}L^3)][ClO_4]_4{\cdot}x MeNO_2{\cdot}yH_2O$ (bottom). All the anions in the top assembly are disordered about crystallographic C_2 axes (not shown), and H atoms are included to highlight its C–H...O interaction. Other details as for Figure 6. Symmetry codes: (iv) 1–*y*, *x*, 1–*z*; (v) *y*, 1–*x*, 1–*z*; (vi) 1–*x*, *y*, $^3/_2$–*z*.

anion is crystallographically ordered, and forms four anion... π interactions and two Ag...O contacts to the cyclic host. The stronger host:guest interaction may compensate energetically for the conformational distortion of the host in this assembly. This more intimate mode of anion binding was not observed in the $[Cu_4(\mu\text{-L})_4]^{4+}$ (L = L^5-L^7) system.[19-21]

A molecular square with a larger anion was also crystallised, namely $[Ag_4(\mu\text{-}L^3)_4][SbF_6]_4{\cdot}MeNO_2$ (monoclinic, $P2_1/n$). The host:guest interactions in this crystal resemble the solvent-free perchlorate salt of that cation, with two SbF_6^- ions forming short anion...π contacts to opposite sides of the host cavity (Figure S26). However, this $[Ag_4(\mu\text{-}L^3)_4]^{4+}$ square adopts a moderately canted conformation, midway between the two forms of its ClO_4^- salt. Moreover, unlike the structures with this mode of ClO_4^- anion association, the SbF_6^- ions are not disordered in the host cavity. Both these differences may reflect the steric properties of the larger SbF_6^- guest anions in that crystal.[30] All the Ag_4 molecular squares form additional anion... π contacts to exogenous ClO_4^- or SbF_6^- ions which, in some cases, bridge between the complex cations in the lattice (Figure S31-S34).

Recrystallisation of $[Ag_4(\mu\text{-}L^3)_4][ClO_4]_4$ from acetonitrile instead yielded mononuclear $[Ag(NCMe)L^3]ClO_4$, containing a planar four-coordinate silver ion with a tridentate L^3 ligand and a slightly bent Ag–NCMe interaction (N{triazinyl}–Ag–N{NCMe} = 167.71(10)°; Figure S35). This is the only compound in this study to show tridentate coordination of L^1-L^4. While (approximately) square planar silver complexes are unusual,[31] comparable geometries are found in some [AgX(terpy)] or [Ag(NCMe)(terpy)]X (terpy = 2,2':6',2''-terpyridine; X^- = anion) derivatives.[32,33] The perchlorate ion does not form any secondary bonding interactions in this structure. A product analysing as $[Ag(NCMe)L^4]ClO_4$ was also isolated, but could not be crystallographically characterised.

Solvent-free $[Ag(\mu\text{-}L^2)]ClO_4$ was phase-pure by powder diffraction, but the solvated silver complex crystals decompose to amorphous powders through solvent loss upon exposure to air. Electrospray mass spectra of all the silver complexes showed peaks corresponding to $[AgL]^+$ and $[AgL_2]^+$ (L = L^2-L^4), with no higher molecular weight species of >5 % abundance. That is common in silver(I) assemblies of heterocyclic N-donor ligands, which can be highly labile in solution.[14,21,33,34]

Since coinage metal complexes of L^5-L^7 have already been described,[19-21] we instead investigated their iron chemistry. Many compounds of type $[Fe(NCE)_2(NN)_2]$ (E = S or Se), where NN is a diimine chelate ligand, exhibit thermal spin-crossover switching properties.[23,35] With that in mind, L^5-L^7 were treated with $Fe[NCS]_2$ or $Fe[NCSe]_2$, which were generated *in situ* in the reaction mixtures. Two different product types were crystallised from these reactions: mononuclear $[Fe(NCS)_2(L^5)_2]$, $[Fe(NCSe)_2(L^5)_2]$ and $[Fe(NCSe)_2(L^6)_2]$; and the coordination polymers $[Fe(NCS)_2(\mu\text{-}L^6)]$, $[Fe(NCS)_2(\mu\text{-}L^7)]$ and $[Fe(NCSe)_2(\mu\text{-}L^7)]$. Different products analysing as $[Fe(NCS)_2(L^5)_2]$ and $[Fe(NCS)_2(L^5)]$ were prepared from appropriate ratios of those metal:ligand precursors, although the latter material was not obtained in single crystal form. Otherwise, the same complex product was isolated from these reactions for a particular ligand and metal reagent, regardless of the metal:ligand ratio used. Mononuclear $[Fe(NCE)_2L_2]$ and polymeric $[Fe(NCE)_2(\mu\text{-L})]$ (L = L^5-L^7) all gave similar electrospray mass spectra, with strong peaks assignable to $[Fe(NCE)L_2]^+$, $[Fe_2(NCE)_3L_2]^+$ and (for L^5 only) $[FeL_3]^{2+}$ species. Hence, we propose that solutions of all these compounds contain mixtures of mononuclear and dinuclear (or higher nuclearity) species, and that the relative solubilities of the mononuclear and polymeric products determine which structure type is isolated in each case.

The mononuclear complexes were characterized as isostructural solvent-free $[Fe(NCS)_2(L^5)_2]$ and $[Fe(NCSe)_2(L^6)_2]$ (triclinic, $P\bar{1}$), and a series of isomorphous solvates $[Fe(NCS)_2(L^5)_2]{\cdot}MeOH$ and $[Fe(NCSe)_2(L^5)_2]{\cdot}solv$ (solv = MeOH, ½EtOH and ½Me_2CO; all monoclinic, $P2_1/n$). The molecular geometry is similar in each case, with *cis* pseudohalide and bidentate heterocyclic ligands (Figure 4). The solvent-free complexes contain one near-linear [Fe–N–C = 170.7(3)-

177.98(16)°] and one bent NCE$^-$ ligand [Fe–N–C = 141.10(15)-158.8(3)°], and heterocyclic ligands that are not perpendicular to each other [Ψ = 104.84(4)-109.94(7)°]. Both these aspects might be expected to favour a high-spin state in those compounds, other things being equal.[36,37] In contrast, the solvated complexes have more similar distributions of Fe–N–C angles between 161.0(2)-169.06(18)°, and 93.18(4) ≤ Ψ ≤ 99.27(4)° which is closer to the ideal value of 90°.

The solvent in the solvate crystals occupies a cavity close to a crystallographic inversion centre, with the ethanol and acetone half-molecules in those solvates being disordered about that special position. The different stoichiometry of those isomorphous crystals presumably reflects that the solvent cavity is large enough to accommodate two molecules of methanol, but only one molecule of ethanol or acetone. Interestingly, the methanol molecule in [Fe(NCS)$_2$(L^5)$_2$]·MeOH donates an O–H...S interaction to a thiocyanate ligand, but the solvent in [Fe(NCSe)$_2$(L^5)$_2$]·MeOH and [Fe(NCSe)$_2$(L^5)$_2$]·½EtOH instead forms an O–H...N hydrogen bond to an uncoordinated L^1 pyrimidyl N-atom (Figures 4, S36 and S37). That may reflect the lower fractional negative charge on the Se atom in the NCSe$^-$ ion, which makes it a weaker hydrogen bond acceptor.[38]

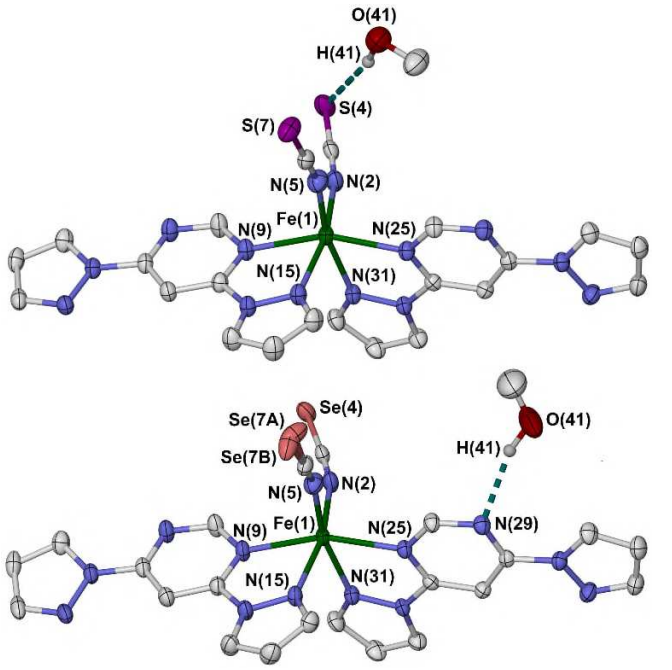

Figure 4 The asymmetric units of [Fe(NCS)$_2$(L^5)$_2$]·MeOH (top) and [Fe(NCSe)$_2$(L^5)$_2$]·MeOH (bottom), showing the different hydrogen bonding in the two isomorphous crystals. Atoms are drawn with 50 % displacement ellipsoids and C-bound H atoms are omitted for clarity. Atom Se(7) in the selenocyanate complex is disordered over two positions. Colour code: C, white; H, pale grey; Fe, green; N, blue; O, red; S, purple; Se, pink.

The molecules in the solvent-free mononuclear complexes associate into stacks through π...π interactions between one pendant pyrazolyl group and its symmetry equivalent, generated by successive crystallographic inversion centres. These stacks are linked into sheets in the (0 $\bar{1}$ 1) crystal plane by a pairwise π...π interaction between the second pendant pyrazolyl group and its symmetry equivalent, *via* another inversion centre. In contrast, the π...π interactions in the solvated crystals are grouped into tetrads, with each molecule participating in two different tetrads oriented approximately perpendicular to each other. This leads to layers of linked molecules in (10$\bar{1}$) plane. Despite these differences, the molecules in both lattices participate in three π...π interactions, forming the same 6^3 network topology of π...π connections.[39]

The three crystalline [Fe(NCE)$_2$(μ-L)] coordination polymers are isomorphous (tetragonal, $I4_1/a$). The main difference between them is that the L^7 amino group in [Fe(NCE)$_2$(μ-L^7)] (E = S, Se) forms intramolecular N–H...N hydrogen bonds to two different NCE$^-$ ligands, which are absent in [Fe(NCS)$_2$(μ-L^6)] (Figure 5). That is also reflected in bending of the pseudohalide ligands, which is more pronounced in the L^7 structures [Fe–N–C = 140.2(4)-141.4(4) and 153.0(5)-155.7(4)°] than in [Fe(NCS)$_2$(μ-L^6)] [Fe–N–C = 152.3(3) and 160.2(3)°]. Other aspects of their molecular structures, including the closest intramolecular Fe...Fe distance [6.3435(2)-6.3590(7)°] and the disposition of the heterocyclic ligands at each iron atom [Ψ = 88.25(8)-88.81(12)°],[35] show only small variation between the compounds. The polymer chains undulate along a crystallographic 4$_1$ screw axis parallel to the *c* direction (Figure 5), and pack *via* a four-fold interdigitation resembling the 'terpyridine embrace' packing motif which is often adopted by complexes of terpyridine and related ligands (Figure S43).[40]

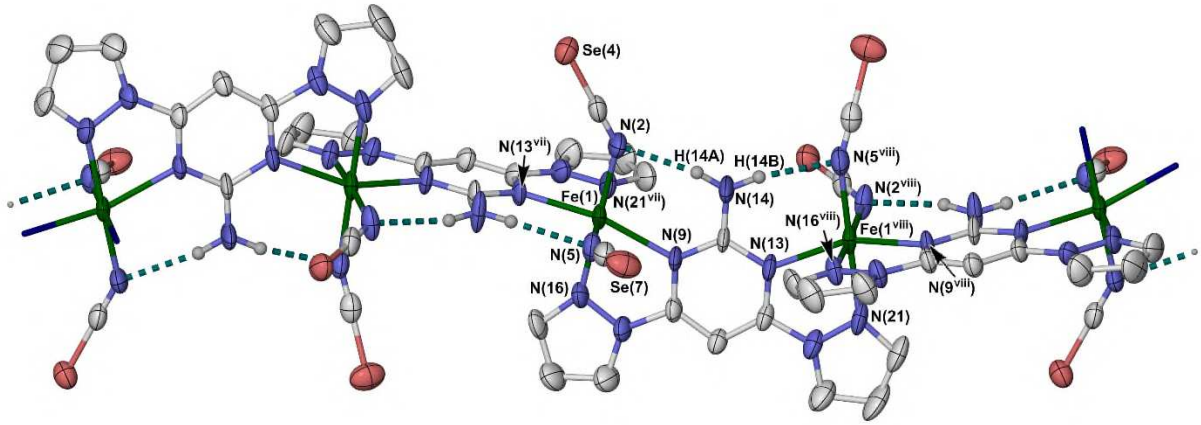

Figure 5 The [Fe(NCSe)$_2$(μ-L^7)] coordination polymer chain. Atoms are drawn with 50 % displacement ellipsoids and C-bound H atoms are omitted for clarity. Colour code: C, white; H, pale grey; Fe, green; N, blue; Se, pink. Symmetry codes: (vii) $^1/_4+y$, $^5/_4-x$, $^1/_4+z$; (viii) $^5/_4-y$, $-^1/_4+x$, $-^1/_4+z$.

Despite their individual structural differences, all these mononuclear compounds and coordination polymers are high-spin at 120 K according to their metric parameters. That was confirmed by magnetic susceptibility data, which showed the compounds mostly remain high-spin between 5-500 K (Figures S44 and S45). However, while they are high-spin when freshly prepared, annealing the $[Fe(NCSe)_2(L^5)_2]$·solv materials generates a new phase showing an abrupt, partial spin-transition at $T_{½}$ = 103 K. The transition reproducibly proceeds to just over 50 % completeness and shows a 6 K thermal hysteresis width, under the conditions of measurement (Figures 6 and S46). Both these aspects may reflect the low temperature of the transition, since cooperative spin transitions with $T_{½} \leq 100$ K can suffer from slow kinetics, trapping a high-spin fraction of the sample below the transition temperature.[41] Unfortunately the $[Fe(NCSe)_2(L^5)_2]$·solv crystals decompose during the annealing process, and the SCO-active phase is not isostructural with solvent-free, high-spin $[Fe(NCS)_2(L^5)_2]$ by powder diffraction (Figure S47). Hence, the structural origin of the spin-transition in $[Fe(NCSe)_2(L^5)_2]$ is presently unclear.

Iron complexes of L^5-L^7 with more weakly coordinating anions crystallised poorly. Only two such compounds were crystallographically characterised, which were 1D coordination polymers with a zig-zag topology. While $[Fe(OCMe_2)(OH_2)(\mu\text{-}L^6)][BF_4]_2 \cdot H_2O$ has all *cis*-coordinated metal nodes,[11] $[Fe(OH_2)_2(\mu\text{-}L^5)][ClO_4]_2$ (monoclinic, *C*2/*c*) has a more complicated structure with alternating *cis*- and *trans*-iron centres (Figure 7). There is extensive, disordered hydrogen bonding between the aqua ligands and ClO_4^- ions, which links the chains into sheets in the (100) plane. This material is also high-spin, as would be expected from its weak-field aqua ligands.

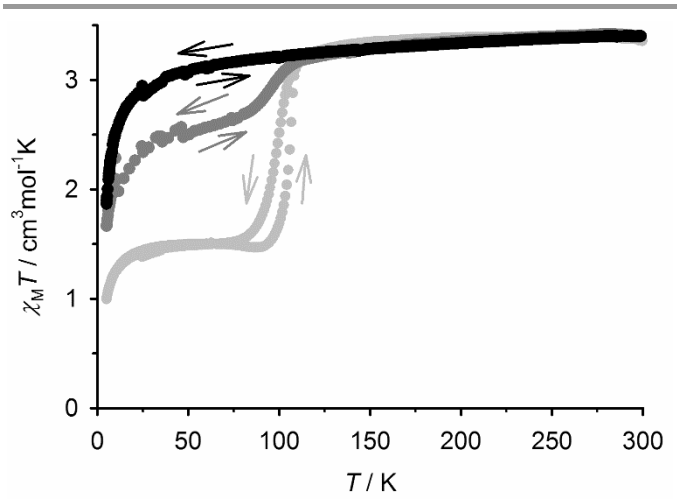

Figure 6 Variable temperature magnetic susceptibility data from $[Fe(NCSe)_2(L^7)_2]$·MeOH, at a scan rate of 5 Kmin^{-1}. Black, freshly prepared material; dark grey, the same sample, after exposure to air for 4 hrs; pale grey; a different sample, annealed at 370 K for 24 hrs.

Conclusions

This study collects together three groups of products, obtained during our further investigations of the coordination chemistry of (potentially) ditopic 2,4-dipyrazolyl-1,3,5-triazine and 4,6-dipyrazolylpyrimidine derivatives.[10,11,13,14] First is the unique cyclic tetramer $[BF_4 \subset \{Fe(L^1)\}_4(\mu\text{-}L^1)_4][BF_4]_7$, which was the unexpected structure of the complex "$[Fe(L^1)_2][BF_4]_2$" (Figure 1).

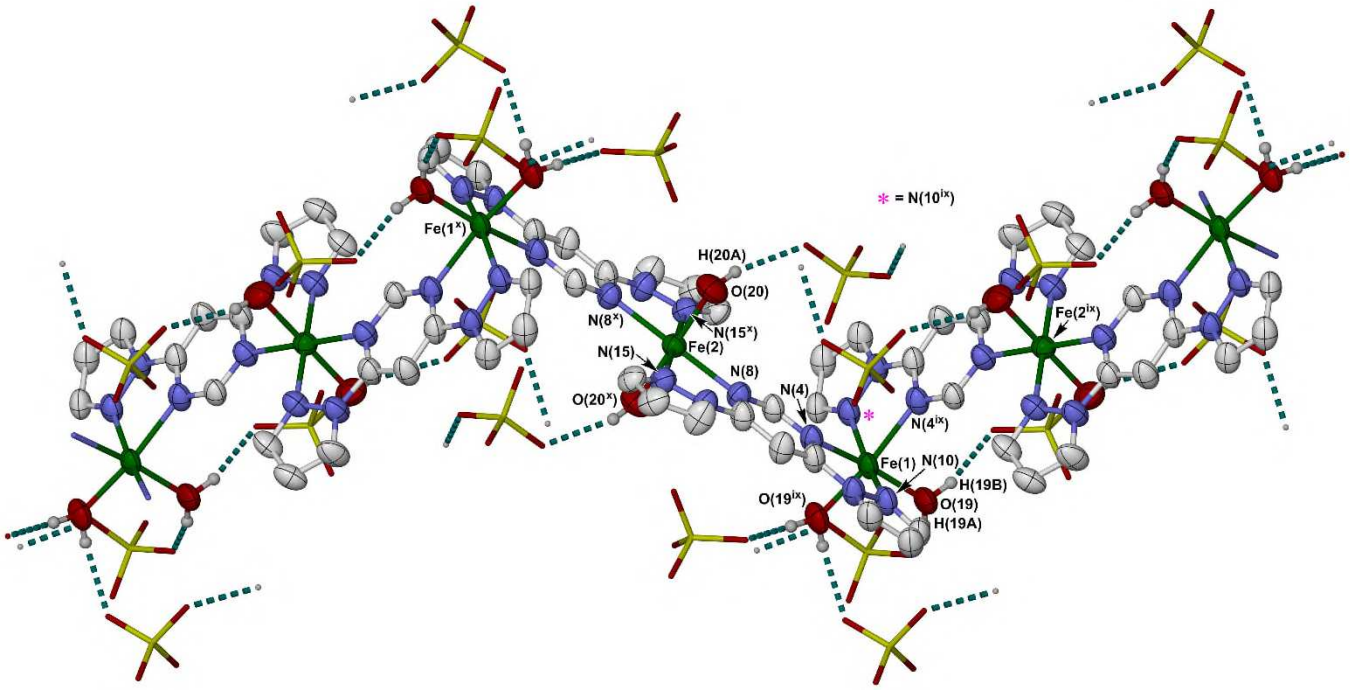

Figure 7 The $[Fe(OH_2)_2(\mu\text{-}L^5)][ClO_4]_2$ coordination polymer chain. Atoms are drawn with 50 % displacement ellipsoids, except for the ClO_4^- ions which are de-emphasised for clarity. Only one orientation of the disordered anions is shown, and C-bound H atoms have been omitted. The aqua ligand atom H(20B) wasn't located in the Fourier map and couldn't be included in the model; it may be disordered between different hydrogen bond acceptor groups (ESI†). Colour code: C, white; H, pale grey; Cl, yellow; Fe, green; N, blue; O, red. Symmetry codes: (ix) 1–*x*, *y*, ½–*z*; (x) 1–*x*, 2–*y*, 1–*z*.

Other homoleptic iron(II) complexes of 2,4-dipyrazolyl-6-R-1,3,5-triazines (R = an amino, alkoxy, sulfanyl or pyrazolyl group)are mononuclear structures,[13] with the tridentate *tris*-heterocycle coordination which is usually adopted by this ligand type.[10,12-14] The alternative preference of the 2,4-dipyrazolyl-6*H*-1,3,5-triazines L^1-L^4 for a *bis*-bidentate coordination mode is also apparent in their silver complexes described below.

The $[\{Fe(L^1)\}_4(\mu\text{-}L^1)_4]^{8+}$ cation was only isolated as its BF_4^- salt, which could reflect the role of the encapsulated BF_4^- ion in templating the metallacycle structure. The part-occupied pyrazole→BF_3 moiety in the lattice, which is a degradation product of the L^1 ligand, might also be required for crystallisation of this compound. The $[\{Fe(L^1)\}_4(\mu\text{-}L^1)_4]^{8+}$ assembly exists in solution, as well as in the solid state, by electrospray mass spectrometry.

Second are the silver complexes which include coordination polymers (Figure 2), molecular squares (Figure 3) and one mononuclear example. The metallacycles resemble the known $[M_4(\mu\text{-}L)_4]^{4+}$ (M = Cu^+ or Ag^+; L = L^5-L^7 or a related ligand) assemblies, in their connectivity and their preferred binding of two anions on either side of their cavity.[19-21] However, a solvate of $[Ag_4(\mu\text{-}L^3)_4][ClO_4]_4$ showed a new, different motif of binding just one anion more intimately at the centre of the assembly, through a larger number of second-sphere contacts. The $[Ag_4(\mu\text{-}L^3)_4]^{4+}$ host molecule distorts its structure significantly to accommodate this alternative mode of anion binding. All the L^1-L^4 assemblies in this study form *intra*-cavity and peripheral anion...π interactions to their anion guests, which are typical for triazinyl anion hosts.[8]

Lastly, iron complexes of the 4,6-dipyrazolylpyrimidines L^5-L^7 are reported, including examples of mononuclear $[Fe(NCE)_2L_2]$ (E = S or Se) complexes (Figure 4) and 1D coordination polymers $[Fe(NCE)_2(\mu\text{-L})]$ (Figure 5). These contain mono- or *bis*-bidentate heterocyclic ligands; L^5-L^7 are geometrically unsuited to tridentate coordination. While complexes of type $[Fe(NCE)_2(NN)_2]$ (NN = a bidentate N-heterocyclic ligand) often exhibit thermal spin-crossover switching properties,[23,35] all the crystalline examples in this work remain high-spin on cooling. That could imply the ligand field exerted by L^5-L^7 is inherently weak, which would favour the high-spin form, or it could be a sterically imposed quenching of spin-crossover by the surrounding lattice.[42] The steric influence of the methyl and amino substituents in L^6 and L^7, which are close to the inner metal coordination sphere, might also favour the longer Fe–N bonds associated with the high-spin state of those complexes.[42]

Intriguingly, a new phase showing a cooperative, low-temperature spin transition was produced by annealing solvated crystals of $[Fe(NCSe)_2(L^5)_2]$ (Figure 6). While this phase could not be structurally characterised, it shows that iron(II)/ L^5 complexes can indeed exhibit spin-crossover under some circumstances. Our current work aims to develop that observation, to produce new spin-crossover molecular materials based on this ligand family.

Experimental

Ligands L^1,[14] L^5,[25] L^6 and L^7 [20] were prepared by the literature procedures. Synthetic procedures and characterisation data for the new ligands L^2-L^4 are given in the ESI†. Other reagents and solvents were purchased commercially and used as supplied.

CAUTION Although we have experienced no problems when using the perchlorate salts in this study, metal-organic perchlorates are potentially explosive and should be handled with care in small quantities.

Synthesis of $[(Fe(L^1)_4(\mu\text{-}L^1)_4][BF_4]_8{\cdot}½PzBF_3$. A solution of L^1 (0.060 g, 0.28 mmol) and $Fe[BF_4]_2{\cdot}6H_2O$ (0.048 g, 0.14 mmol) in MeCN (5 cm^3) was stirred at room temperature until all the solid had dissolved. Addition of diethyl ether to the filtered solution afforded the product as a yellow powder. Orange single crystals of the tetrameric complex were grown by slow evaporation of an acetonitrile solution of the compound. Yield 0.067 g, 74 %. Elemental analysis: found C, 33.0; H, 2.30; N, 29.3 %. Calcd for Calcd for $C_{72}H_{56}Fe_4N_{56}B_8F_{32}{\cdot}½C_3H_4N_2BF_3$: C, 32.8; H, 2.17; N, 29.7 %. ESMS *m/z* 214.1 (81, $[HL^1]^+$), 236.1 (73, $[Na(L^1)]^+$), 241.1 (60, $[Fe(L^1)_2]^{2+}$), 288.1 (85, $[Fe(L^1)F]^+$), 449.1 (15, $[Na(L^1)_2]^+$), 501.1 (100, $[Fe(L^1)_2F]^+$), 569.1 (2, $[Fe(L^1)_2BF_4]^+$), 572.3 (5, $[Fe(L^1)_2(O_2CH)_2]^+$), 594.6 (4, $[FeNa(L^1)_5(O_2CH)]^{2+}$), 944.1 (3, $[Fe_2Na(L^1)_7(BF_4)_3]^{2+}$), 1225.2 (5, $[Fe_4(L^1)_8(BF_4)_6]^{2+}$). ^1H NMR (CD_3NO_2) δ 11.0 (2H, Trz H^6), 39.5 and 42.1 (both 4H, Pz H^3 + H^5), 70.4 (4H, Pz H^4).

We have written the formula of this compound to include the half-equivalent pyrazole→BF_3 adduct (Figure 1). While the microanalysis fit is slightly improved with that formulation, the elemental compositions of the material including or lacking this moiety are identical within the error of the measurement.

Synthesis of *catena*-$[Ag(\mu\text{-}L^2)]ClO_4$. A mixture of $AgClO_4$ (0.014 g, 0.08 mmol) and L^2 (0.023 g, 0.08 mmol) in nitromethane (5 cm^3) was stirred until all the solid had dissolved. The solution was concentrated to *ca* half its original volume, then filtered. Slow diffusion of diethyl ether vapour into the solution yielded pale yellow crystals of the product. The solution was kept in the dark during the crystallisation process. Yield 0.022 g, 56 %. Elemental analysis: found C, 22.2; H, 0.96; N, 20.1 %. Calcd for $C_9H_5AgCl_3N_7O_4$: C, 22.1; H, 1.03; N, 20.0 %. ESMS *m/z* 389.8987 (calcd for $[Ag(L^2)]^+$ 387.9029), 670.8954 (calcd for $[Ag(L^2)_2]^+$ 668.9012).

Synthesis of *catena*-$[Ag(NCMe)(\mu\text{-}L^2)]ClO_4$. The previous reaction, carried out under the same conditions using acetonitrile as the solvent, afforded this off-white crystalline product. Yield 0.017 g, 40 %. The crystals decomposed to an off-white powder upon drying *in vacuo*, implying loss of acetonitrile from the material. That was confirmed by microanalysis, which supported an approximate formula of $[Ag(NCMe)_{0.25}(L^2)]ClO_4$. Elemental analysis: found C, 22.4; H, 1.38; N, 20.4 %. Calcd for $C_{9.5}H_{5.75}AgCl_3N_{7.25}O_4$: C, 22.8; H, 1.16; N, 20.3 %.

Synthesis of $[Ag_4(\mu\text{-}L^3)_4][ClO_4]_4$. Method as for $[Ag(\mu\text{-}L^2)]ClO_4$, using L^3 (0.021 g, 0.08 mmol). The product formed colourless crystals from nitromethane/diethyl ether, in a mixture of (solvated) needle and (solvent-free) cubic morphologies which were both crystallographically characterised. The needle form predominated in most crystallisation vials. Yield 0.024 g, 62 %. Elemental analysis: found C, 32.8; H, 3.06; N, 20.7 %. Calcd for $C_{52}H_{60}Ag_4Cl_4N_{28}O_{16}$: C, 32.8; H, 3.17; N, 20.6 %. ESMS *m/z* 376.0409 (calcd for $[Ag(L^3)]^+$ 376.0434), 645.1792 (calcd for $[Ag(L^3)_2]^+$ 645.1823).

Synthesis of $[Ag(NCMe)(L^3)]ClO_4$. The above reaction, carried out under the same conditions using acetonitrile as the solvent, yielded crystals of this mononuclear complex. Elemental analysis: found C, 39.2; H, 3.71; N, 24.5 %. Calcd for $C_{15}H_{18}AgClN_8$: C, 39.7; H, 4.00; N, 24.7 %.

Synthesis of $[Ag_4(\mu\text{-}L^3)_4][SbF_6]_4$. Method as for $[Ag(\mu\text{-}L^2)]ClO_4$, using $AgSbF_6$ (0.028 g, 0.08 mmol) and L^3 (0.021 g, 0.08 mmol). Slow diffusion of diethyl ether vapour into the supernatant at –20 °C gave the product as colourless needles. Yield 0.012 g, 24 %. Elemental analysis: found C, 25.7; H, 2.32; N, 16.2 %. Calcd for $C_{52}H_{60}Ag_4F_{24}N_{28}Sb_4$: C, 25.5; H, 2.47; N, 16.0 %.

Synthesis of $[Ag_4(\mu\text{-}L^4)_4][ClO_4]_4$. Method as for $[Ag(\mu\text{-}L^2)]ClO_4$, using L^4 (0.026 g, 0.08 mmol). Slow diffusion of diethyl ether into the resultant nitromethane solution yielded a white powder of unknown composition, mixed with some colourless needles of the nitromethane solvate of the title compound. Limited characterisation was achieved from crystals isolated from the mixture by a Pasteur separation, but the complex was not obtained in analytical purity. Yield 0.008 g, 19 %. ESMS *m/z* 428.0700 (calcd for $[Ag(L^4)]^+$ 428.0747), 749.2408 (calcd for $[Ag(L^4)_2]^+$ 749.2449).

Synthesis of $[Ag(NCMe)(L^4)]ClO_4$. The above reaction, carried out in acetonitrile yielded a product analysing as $[Ag(NCMe)L^4]ClO_4$, which was not crystallographically characterised. Yield 0.019 g, 42 %. Elemental analysis: found C, 40.3; H, 3.79; N, 19.5 %. Calcd for $C_{19}H_{22}AgClN_8O_4$: C, 40.1; H, 3.89; N, 19.7 %.

Synthesis of $[Fe(NCS)_2(L^5)_2]$. Separate solutions of $Fe[ClO_4]_2{\cdot}6H_2O$ (0.034 g, 0.094 mmol) and KNCS (0.018 g, 0.19 mmol) in methanol (2 x 3 cm^3) were mixed, and stirred at room temperature for 5 mins. The resultant suspension was centrifuged, and a solution of L^5 (0.040 g, 0.19 mmol) in methanol (3 cm^3) was then added. Slow evaporation of the solvent from the filtered mixture led to red single crystals of the product. Yield 0.048 g, 85 %. Elemental analysis: found C, 44.2; H, 2.75; N, 32.7 %. Calcd for $C_{22}H_{16}N_{14}FeS_2$ C, 44.3; H, 2.70; N, 32.9 %. ESMS *m/z* 240.1 $[Fe(L^5)_2]^{2+}$, 346.1 $[Fe(L^5)_3]^{2+}$, 538.1 $[Fe(L^5)_2(NCS)]^+$, 710.0 $[Fe_2(L^5)_2(NCS)_3]^+$.

Synthesis of *catena*-$[Fe(NCS)_2(\mu\text{-}L^5)]$. Method as for $[Fe(NCS)_2(L^5)_2]$, using half the amount of L^5 (0.020 g, 0.094 mmol). Slow evaporation of the solution yielded red crystals of the product. Yield 0.019 g, 53 %. Elemental analysis: found C, 37.6; H, 2.23; N, 29.2 %. Calcd for $C_{12}H_8FeN_8S_2$ C, 37.5; H 2.10; N, 29.2 %.

Synthesis of *catena*-$[Fe(NCS)_2(\mu\text{-}L^6)]$. Method as for $[Fe(NCS)_2(L^5)_2]$, using L^6 (0.021 g, 0.094 mmol). Slow evaporation of the solution yielded red crystals of the product. Yield 0.008 g, 21 %. Elemental analysis: found C, 39.3; H, 2.62; N, 28.2 %. Calcd for $C_{13}H_{10}N_8FeS_2$: C, 39.2; H, 2.53; N, 28.1 %. ESMS *m/z* 566.2 $[Fe(L^6)_2(NCS)]^+$, 738.1 $[Fe_2(L^6)_2(NCS)_3]^+$.

Synthesis of *catena*-$[Fe(NCS)_2(\mu\text{-}L^7)]$. Method as for $[Fe(NCS)_2(L^5)_2]$, using L^7 (0.021 g, 0.094 mmol). The product was a red crystalline solid. Yield 0.029 g, 78 %. Elemental analysis: found C, 36.2; H, 2.21; N, 31.5 %. Calcd for $C_{12}H_9N_9FeS_2$: C, 36.1; H, 2.27; N, 31.6 %. ESMS *m/z* 568.2 $[Fe(L^7)_2(NCS)]^+$, 740.1 $[Fe_2(L^7)_2(NCS)_3]^+$.

Synthesis of $[Fe(NCSe)_2(L^5)_2]$. Separate solutions of $Fe[ClO_4]_2{\cdot}6H_2O$ (0.024 g, 0.066 mmol) and KNCSe (0.019 g, 0.13 mmol) in methanol (2 x 3 cm^3) were mixed, and stirred at room temperature for 5 mins. The resultant suspension was centrifuged, and a solution of L^5 (0.029 g, 0.13 mmol) in methanol (3 cm^3) was then added. Slow evaporation of the solvent from the filtered mixture led to yellow single crystals of formula $[Fe(NCSe)_2(L^1)_2]{\cdot}MeOH$, which analysed as the solvent-free complex after drying *in vacuo*. Yield 0.048 g, 37 %. Elemental analysis: found C, 38.4; H, 2.53; N, 28.3 %. Calcd for $C_{22}H_{16}N_{14}FeSe_2$: C, 38.3; H, 2.34; N, 28.4 %. ESMS *m/z* 240.1 $[Fe(L^5)_2]^{2+}$, 346.1 $[Fe(L^5)_3]^{2+}$, 373.9 $[Fe(L^5)(NCSe)]^+$, 391.9 $[Fe(L^5)(NCSe)(H_2O)]^+$.

The same procedure using ethanol or acetone as solvent afforded the isomorphous crystalline solvates $[Fe(NCSe)_2(L^5)_2]{\cdot}½EtOH$ and $[Fe(NCSe)_2(L^5)_2]{\cdot}½Me_2CO$.

Synthesis of $[Fe(NCSe)_2(L^6)_2]$. Method as for $[Fe(NCSe)_2(L^5)_2]$, using L^6 (0.030 g, 0.13 mmol). Slow evaporation of the solution yielded yellow crystals of the product. Yield 0.026 g, 27 %. Elemental analysis: found C, 40.0; H, 2.85; N, 27.1 %. Calcd for $C_{24}H_{20}N_{14}FeSe_2$: C, 40.1; H, 2.81; N, 27.3 %. ESMS *m/z* 614.2 $[Fe(L^6)_2(NCSe)]^+$, 881.9 $[Fe_2(L^6)_2(NCSe)_3]^+$.

Synthesis of *catena*-$[Fe(NCSe)_2(\mu\text{-}L^7)]$. Method as for $[Fe(NCSe)_2(L^5)_2]$, using L^7 (0.015 g, 0.066 mmol). Slow evaporation of the solution yielded yellow crystals of the product. Yield 0.021 g, 64 %. Elemental analysis: found C, 29.3; H, 1.75; N, 25.4 %. Calcd for $C_{12}H_9N_9FeSe_2$: C, 29.2; H, 1.84; N, 25.6 %. ESMS *m/z* 616.2 $[Fe(L^7)_2(NCSe)]^+$, 883.9 $[Fe_2(L^7)_2(NCSe)_3]^+$.

Synthesis of *catena*-$[Fe(OH_2)_2(\mu\text{-}L^5)][ClO_4]_2$. A mixture of $Fe[ClO_4]_2{\cdot}6H_2O$ (0.051 g, 0.14 mmol) and L^5 (0.030 g, 0.14 mmol) in nitromethane (4 cm^3) was stirred until all the solid had dissolved. The yellow solution was then filtered. Slow evaporation of the solvent yielded yellow crystals of the product, which were collected and analysed without further purification. Yield 0.067 g, 94 %. Elemental analysis: found C,

23.6; H, 2.36; N, 16.6 %. Calcd for $C_{10}H_{12}N_6FeO_{10}Cl_2$ C, 23.9; H, 2.40; N, 16.7 %.

A second coordination polymer $[Fe(OCMe_2)(OH_2)(\mu\text{-}L^6)][BF_4]_2{\cdot}H_2O$ was also crystallised during this study, and has been described elsewhere.[11]

Single Crystal Structure Analyses

Diffraction data for $[Fe(NCS)_2(\mu\text{-}L^7)]$ were recorded at station I19 of the Diamond synchrotron (λ = 0.6889 Å). All other crystallographic data were measured with an Agilent Supernova dual-source diffractometer using monochromated Cu-K_α (λ = 1.5418 Å) or Mo-K_α (λ = 0.7107 Å) radiation. The diffractometer was fitted with an Oxford Cryostream low-temperature device. All the structures were solved by direct methods *(SHELXS97*[43]), and developed by full least-squares refinement on F^2 (*SHELXL97*[43]). Crystallographic figures were prepared using *XSEED*,[44] and octahedral coordination volumes (V_{Oh}) were calculated with *Olex2*.[45]

Experimental details for the structure are listed in Tables S1 and S2, while details of the crystallographic refinements are also given in the ESI†.

Other measurements

Elemental microanalyses were performed by the microanalytical services at the University of Leeds School of Chemistry, or the London Metropolitan University School of Human Sciences. Electrospray mass spectra were recorded on a Bruker MicroTOF-q instrument, from chloroform solution (organic compounds) or nitromethane solution (metal complexes). Any sodium- and formate-containing species in the mass spectra originate from the sodium formate calibrant used. Diamagnetic NMR spectra employed a Bruker DPX300 spectrometer operating at 300.1 MHz (^{1}H) or 75.5 MHz (^{13}C), while paramagnetic NMR spectra used a Bruker Ascend400 (400.1 MHz) spectrometer. X-ray powder diffraction patterns were measured using a Bruker D2 Phaser diffractometer.

Solid state magnetic susceptibility measurements were performed on a Quantum Design SQUID/VSM magnetometer, with an applied field of 5000 G and a scan rate of 5 Kmin^{-1}. A diamagnetic correction for the sample was estimated from Pascal's constants;[46] a diamagnetic correction for the sample holder was also applied.

Conflicts of interest

There are no conflicts to declare.

Acknowledgements

The authors thank Dr. O. Cespedes and S. A. Barrett (University of Leeds) for help with the solid state and solution phase magnetic measurements. This work was funded by the Leverhulme Trust (RPG-2015-095), the EPSRC (EP/K012568/1, EP/K00512X/1) and the University of Leeds. We thank Diamond Light Source for access to beamline I19 (MT10334), which contributed to the results presented here.

Notes and references

¶The N–B bond in the pyrazole→BF_3 half-molecule is N(173)–B(178) = 1.629(18) Å (Figure 1). For comparison, the N–B distances in the literature structure $S(\{F_3B\}C_3H_3N_2\text{-}1,2)_2$ are 1.601(2) and 1.629(3) Å.[27]

1 H. T. Chifotides and K. R. Dunbar, *Acc. Chem. Res.*, 2013, **46**, 894; D. A. Safin, J. M. Frost and M. Murugesu, *Dalton Trans.*, 2015, **44**, 20287.
2 L. K. Thompson and L. N. Dawe, *Coord. Chem. Rev.*, 2015, **289–290**, 13.
3 L. N. Dawe, K. V. Shuvaev and L. K. Thompson, *Chem. Soc. Rev.*, 2009, **38**, 2334; J. G. Hardy, *Chem. Soc. Rev.,* 2013, **42**, 7881.
4 Y. Inokuma, M. Kawano and M. Fujita, *Nature Chem.*, 2011, **3**, 349; B. Therrien, *J. Organomet. Chem.*, 2011, **696**, 637.
5 See *eg* D. Sun, S. Ma, Y. Ke, D. J. Collins and H.-C. Zhou, *J. Am. Chem. Soc.*, 2006, **128**, 3896; Y. K. Park, S. B. Choi, H. Kim, K. Kim, B.-H. Won, K. Choi, J.-S. Choi, W.-S. Ahn, N. Won, S. Kim, D. H. Jung, S.-H. Choi, G.-H. Kim, S.-S. Cha, Y. H. Jhon and J. K. Yang, *Angew. Chem., Int. Ed.*, 2007, **46**, 8230; B. Li, Z. Zhang, Y. Li, K. Yao, Y. Zhu, Z. Deng, F. Yang, X. Zhou, G. Li, H. Wu, N. Nijem, Y. J. Chabal, Z. Lai, Y. Han, Z. Shi, S. Feng, and J. Li, *Angew. Chem., Int. Ed.*, 2012, **51**, 1412; D. Tian, Q. Chen, Y. Li, Y.-H. Zhang, Z. Chang and X.-H. Bu, *Angew. Chem., Int. Ed.*, 2014, **53**, 837; X. Zhao, X. Bu, E. T. Nguyen, Q.-G. Zhai, C. Mao and P. Feng, *J. Am. Chem. Soc.*, 2016, **138**, 15102; Y. Zhang, X.-Q. Meng, H.-J. Ding, X. Wang, M.-H. Yu, S.-M. Zhang, Z. Chang and X.-H. Bu, *ACS Appl. Mater. Interf.*, 2019, **11**, 20995.
6 K. Rissanen, *Chem. Soc. Rev.*, 2017, **46**, 2638.
7 D.-S. Zhang, Q. Gao, Z. Chang, X.-T. Liu, B. Zhao, Z.-H. Xuan, T.-L. Hu, Y.-H. Zhang, J. Zhu and X.-H. Bu, *Adv. Mater.*, 2018, **30**, 1804715.
8 P. Gamez and J. Reedijk, *Eur. J. Inorg. Chem.*, 2006, 29; M. Giese, M. Albrecht and K. Rissanen, *Chem. Commun.,* 2016, **52**, 1778; A. Bauzá, T. J. Mooibroek and A. Frontera, *CrystEngComm*, 2016, **18**, 10.
9 M. A. Halcrow, *Coord. Chem. Rev.*, 2009, **253**, 2493; L. J. Kershaw Cook, R. Mohammed, G. Sherborne, T. D. Roberts, S. Alvarez and M. A. Halcrow, *Coord. Chem. Rev.*, 2015, **289–290**, 2.
10 I. Capel Berdiell, A. N. Kulak, S. L. Warriner and M. A. Halcrow, *ACS Omega*, 2018, **3**, 18466.
11 I. Capel Berdiell, C. Desplanches, T. Hochdörffer, R. Kulmaczewski, J. A. Wolny, S. L. Warriner, O. Cespedes, V. Schünemann, G. Chastanet and M. A. Halcrow, under revision.
12 See *eg* R. Hao, M. Li, Y. Wang, J. Zhang, Y. Ma, L. Fu, X. Wen, Y. Wu, X. Ai, S. Zhang and Y. Wei, *Adv. Funct. Mater.*, 2007, **17**, 3663; M. I. J. Stich, M. Schaeferling and O. S. Wolfbeis, *Adv. Mater.*, 2009, **21**, 2216; D. Quiñonero, P. M. Deyà, M. P. Carranza, A. M. Rodríguez, F. A. Jalón and B. R. Manzano, *Dalton Trans.*, 2010, **39**, 794; M. P. Carranza, B. R. Manzano, F. A. Jalón, A. M. Rodríguez, L. Santos and M. Moreno, *Inorg. Chem.*, 2010, **49**, 3828; G. Shao, R. Han, Y. Ma, M. Tang, F. Xue, Y. Sha and Y. Wang, *Chem. Eur. J.*, 2010, **16**, 8647; C. Yang, O. Elbjeirami, C. S. P. Gamage, H. V. R. Dias and M. A. Omary, *Chem. Commun.*, 2011, **47**, 7434; C. Di Nicola, F. Garau, F. Marchetti, M. Monari, L. Pandolfo, C. Pettinari, and A. Venzo, *Dalton Trans.*, 2011, **40**, 4941; W.-S. Lo, J. Zhang, W.-T. Wong and G.-L. Law, *Inorg. Chem.*, 2015, **54**, 3725.
13 I. Capel Berdiell, R. Kulmaczewski and M. A. Halcrow, *Inorg. Chem.*, 2017, **56**, 8817.
14 I. Capel Berdiell, S. L. Warriner and M. A. Halcrow, *Dalton Trans.*, 2018, **47**, 5269.
15 M. Privman and P. Zuman, *Heterocycles*, 1994, **37**, 1637; M. M. Turnbull, M. Y. Wei and R. D. Willett, *J. Coord. Chem.*, 1995, **35**, 11; P. Paul, B. Tyagi, M. M. Bhadbhade and

E. Suresh, *J. Chem. Soc., Dalton Trans.*, 1997, 2273; X.-P. Zhou, D. Li, S.-L. Zheng, X. Zhang and T. Wu, *Inorg. Chem.*, 2006, **45**, 7119; J. Manzur, C. Acuña, A. Vega and A. M. García, *Inorg. Chim. Acta*, 2011, **374**, 637.
16 R. Uson, L. A. Oro, M. Esteban, D. Carmona, R. M. Claramunt and J. Elguero, *Polyhedron*, 1984, **2**, 213; K. T. Prasad, B. Therrien, S. Geib and K. M. Rao, *J. Organomet. Chem.*, 2010, **695**, 495.
17 F. Gómez-de la Torre, A. de la Hoz, F. A. Jalón, B. R. Manzano, A. M. Rodríguez, J. Elguero and M. Martínez-Ripoll, *Inorg. Chem.*, 2000, **39**, 1152.
18 J. Elguero, A. Guerrero, F. Gómez-de la Torre, A. de la Hoz, F. A. Jalón, B. R. Manzano and A. Rodríguez, *New J. Chem.*, 2001, **25**, 1050.
19 B. R. Manzano, F. A. Jalón, I. M. Ortiz, M. L. Soriano, F. Gómez de la Torre, J. Elguero, M. A. Maestro, K. Mereiter and T. D. W. Claridge, *Inorg. Chem.*, 2008, **47**, 413.
20 M. I. Ortiz, M. L. Soriano, M. P. Carranza, F. A. Jalón, J. W. Steed, K. Mereiter, A. M. Rodríguez, D. Quiñonero, P. M. Deyà and B. R. Manzano, *Inorg. Chem.*, 2010, **49**, 8828.
21 M. C. Carrión, I. M. Ortiz, F. A. Jalón, B. R. Manzano, A. M. Rodríguez and J. Elguero, *Cryst. Growth Des.*, 2011, **11**, 1766.
22 V. Patroniak, A. R. Stefankiewicz, J.-M. Lehn and M. Kubicki, *Eur. J. Inorg. Chem.*, 2005, 4168.
23 N. F. Sciortino and S. M. Neville, *Aust. J. Chem.*, 2014, **67**, 1553.
24 Recent general reviews of spin-crossover materials: K. S. Kumar and M. Ruben, *Coord. Chem. Rev.*, 2017, **346**, 176; G. Molnár, S. Rat, L. Salmon, W. Nicolazzi and A. Bousseksou, *Adv. Mater.*, 2018, **30**, 17003862; J. Zarembowitch, F. Varret, A. Hauser, J. A. Real and K. Boukheddaden, *C. R. Chimie*, 2018, **21**, 1056.
25 P. J. Steel and E. C. Constable, *J. Chem. Res. (S)*, 1989, 189.
26 J.-X. Wang, C. Wang, X. Wang, X.-Y. Wang, Y.-H. Xing and Q. Sun, *Spectrochim. Acta, Part A*, 2015, **142**, 55.
27 E. Lork and R. Mews, *Z. Anorg. Allg. Chem.*, 2005, **631**, 1609.
28 T. J. Mooibroek, S. J. Teat, C. Massera, P. Gamez and J. Reedijk, *Cryst. Growth Des.*, 2006, **6**, 1569.
29 A. W. Addison, T. N. Rao, J. Reedijk, J. van Rijn and G. C. Verschoor, *J. Chem. Soc., Dalton Trans.*, 1984, 1349.
30 D. M. P. Mingos and A. L. Rohl, *J. Chem. Soc., Dalton Trans.*, 1991, 3419.
31 A. G. Young and L. R. Hanton, *Coord. Chem. Rev.*, 2008, **252**, 1346.
32 See *eg* S. bin Silong, J. D. Kildea, W. Patalinghug, B. W. Skelton and A. H. White, *Aust. J. Chem.*, 1994, **47**, 1545; E. C. Constable, A. J. Edwards, G. R. Haire, M. J. Hannon and P. R. Raithby, *Polyhedron*, 1998, **17**, 243; G. Baum, E. C. Constable, D. Fenske, C. E. Housecroft, T. Kulke, M. Neuburger and M. Zehnder, *J. Chem. Soc., Dalton Trans.*, 2000, 945; L. Hou, D. Li, Y. G. Yin, T. Wu and S. W. Ng, *Acta Crystallogr., Sect. E: Struct. Rep. Online*, 2004, **60**, m1106; S. Sharma, G. J. E. Davidson and S. J. Loeb, *Chem. Commun.*, 2008, 582; J. E. Aguado, M. C. Gimeno, P. G. Jones and A. Laguna, *Can. J. Chem.*, 2009, **87**, 341.
33 M. J. Hannon, C. L. Painting, E. A. Plummer, L. J. Childs and N. W. Alcock, *Chem. Eur. J.*, 2002, **8**, 2226.
34 R. Zibaseresht and R. M. Hartshorn, *Dalton Trans.*, 2005, 3898; G. M. Borrajo-Calleja, E. de Julián, E. Bayón, J. Díez, E. Lastra, I. Merino and M. P. Gamasa, *Inorg. Chem.*, 2016, **55**, 8794.
35 P. Guionneau, M. Marchivie, G. Bravic, J.-F. Létard and D. Chasseau, *Top. Curr. Chem.*, 2004, **234**, 97; M. A. Halcrow, *Polyhedron*, 2007, **26**, 3523; H. L. C. Feltham, A. S. Barltrop and S. Brooker, *Coord. Chem. Rev.*, 2017, **344**, 26.
36 H. J. Shepherd, T. Palamarciuc, P. Rosa, P. Guionneau, G. Molnár, J.-F. Létard and A. Bousseksou, *Angew. Chem., Int. Ed.*, 2012, **51**, 3910.
37 S. Rodríguez-Jiménez and S. Brooker, *Inorg. Chem.*, 2017, **56**, 13697.
38 P. W. Schultz, G. E. Leroi and J. F. Harrison, *Mol. Phys.*, 1996, **88**, 217.
39 L. Öhrström and K. Larsson, Molecule-Based Materials – the Structural Network Approach, Elsevier, Amsterdam, 2005, p. 314.
40 I. Dance and M. Scudder, *CrystEngComm*, 2009, **11**, 2233.
41 See *eg* G. Ritter, E. König, W. Irler and H. A. Goodwin, *Inorg. Chem.*, 1978, **17**, 224; V. A. Money, C. Carbonera, J. Elhaïk, M. A. Halcrow, J. A. K. Howard and J.-F. Létard, *Chem. Eur. J.*, 2007, **13**, 5503; Y. Garcia, V. Ksenofontov, S. Mentior, M. Dirtu, C. Gieck, A. Bhatthacharjee and P. Gütlich, *Chem. Eur. J.*, 2008, **14**, 3745; J.-F. Létard, S. Asthana, H. J. Shepherd, P. Guionneau, A. E. Goeta, N. Suemura, R. Ishikawa and S. Kaizaki, *Chem. Eur. J.*, 2012, **18**, 5924; N. Paradis, G. Chastanet, F. Varret and J.-F. Létard, *Eur. J. Inorg. Chem.*, 2013, 968.
42 M. A. Halcrow, *Chem. Soc. Rev.*, 2011, **40**, 4119.
43 G. M. Sheldrick, *Acta Cryst. Sect. C.: Struct. Chem.*, 2015, **71**, 3.
44 L. J. Barbour, *J. Supramol. Chem.*, 2001, **1**, 189.
45 O. V. Dolomanov, L. J. Bourhis, R. J. Gildea, J. A. K. Howard and H. Puschmann, *J. Appl. Cryst.*, 2009, **42**, 339.
46 C. J. O'Connor, *Prog. Inorg. Chem.*, 1982, **29**, 203.